Spontaneous liquid water dissociation on hybridised boron nitride and graphene atomic layers from ab initio molecular dynamics simulations

Benoit Grosjean, Anton Robert, Rodolphe Vuilleumier, Marie-Laure Bocquet

PCCP
Physical Chemistry Chemical Physics

Accepted Manuscript

This article can be cited before page numbers have been issued, to do this please use: B. Grosjean, A. Robert, R. Vuilleumier and M. L. Bocquet, *Phys. Chem. Chem. Phys.*, 2020, DOI: 10.1039/C9CP06765E.

This is an Accepted Manuscript, which has been through the Royal Society of Chemistry peer review process and has been accepted for publication.

Accepted Manuscripts are published online shortly after acceptance, before technical editing, formatting and proof reading. Using this free service, authors can make their results available to the community, in citable form, before we publish the edited article. We will replace this Accepted Manuscript with the edited and formatted Advance Article as soon as it is available.

You can find more information about Accepted Manuscripts in the Information for Authors.

Please note that technical editing may introduce minor changes to the text and/or graphics, which may alter content. The journal's standard Terms & Conditions and the Ethical guidelines still apply. In no event shall the Royal Society of Chemistry be held responsible for any errors or omissions in this Accepted Manuscript or any consequences arising from the use of any information it contains.

ROYAL SOCIETY OF CHEMISTRY

rsc.li/pccp

View Article Online
DOI: 10.1039/C9CP06765E

Spontaneous Liquid Water Dissociation on Hybridised Boron Nitride and Graphene atomic layers from Ab Initio Molecular Dynamics Simulations

Benoît Grosjean,[1] Anton Robert,[1] Rodolphe Vuilleumier,[1] and Marie-Laure Bocquet[1,*]

[1] *PASTEUR, Département de chimie, École normale supérieure, PSL University, Sorbonne Université, CNRS, 75005 Paris, France*

Abstract

Two-dimensional materials such as graphene (G) and hexagonal boron nitride (BN) have demonstrated potential applications in membrane science and in particular for the harvest of blue energy. Although pure G and BN atomic layers are known to remain inert towards neutral water, one may wonder about the aqueous reactivity of hybridized monolayers formed by joining BN and G sheets in a planar fashion. Here, we perform Ab Initio molecular dynamics of liquid water in contact with all possible planar heterostructures. Remarkably, we could observe the spontaneous chemisorption and dissociation of interfacial water molecule into its self-ions, at one specific and non-standard one-dimensional border. Our simulations predict that this type of heterostructure is prone to ionize liquid water already in the absence of any electrical gating.

* Correspondence and request for materials should be addressed to M.-L. B. (marie-laure.bocquet@ens.fr)

View Article Online
DOI: 10.1039/C9CP06765E

INTRODUCTION

Among the many materials being studied for chemical applications, two-dimensional (2D) ideal materials like graphene (G hereafter) and hexagonal boron nitride (hBN; BN hereafter) are some of the most versatile and interesting ones, thanks to their structural similarity albeit differential properties and especially for BN to its promising applications in blue energy - harvesting energy from salinity gradient in water [1, 2]. However less is known about how doping in these twin materials alters their interactions with interfacial molecules. Indeed, experimental routes to produce hybrid composites of BN and G have been pioneered by Ci and coworkers [3] and recently summarized in a review [4]. Precisely several routes of synthesis have emerged either from bulk copolymerisation [5] or from growing catalytically on a variety of pure and alloy metal substrates, such as Cu [6–10], Ru [11–13], Rh [14], Ir [15, 16], Pt[17] or Cu-Ni alloy [18]. The latter fabrication of metal-supported monolayers are being obtained with high levels of control being reported on the nanometer scale thanks to the Scanning Tunneling Microscopy (STM) probe and sometimes real-time Low Energy Electron Microscopy (LEEM). In most of these studies, zigzag (ZZ) linking edges are preferentially formed with respect to the armchair (AC) interface. Moreover in the ZZ edge there is either a C-N interface or a C-B interface - defining donor and acceptor interface states respectively -, the latter being found more favorable [15].

Beyond synthesis and characterisation, there is much less progress on the reactivity of the as produced composite border. Using zero Kelvin DFT framework the dissociative reactivity of a gaseous molecules such as di-oxygen [5, 19] and water [20] have been explored on a variety of hybridised materials issued from G and BN. But the reacting molecules were always treated as single frozen species, far from their true environment in the liquid water. Indeed liquid water requires a full quantum treatment to properly include dynamical proton transfers between H-bonding water molecules denoted as the Grotthuss mechanism.[21–23] Closer to the task at hand, M. Sprik has shown in pioneering publications that the full quantum treatment of interfacial water is necessary for correctly describing the proton state at wet surfaces of oxide and clay materials. [24, 25] To our knowledge, a realistic simulation of the interface between water solvent and in-plane BN-G heterostructures remains highly promising albeit challenging. This is the major goal of our study.

View Article Online
DOI: 10.1039/C9CP06765E

From our comparative theoretical study of suspended G and BN monolayers immersed into high pH ionized water [26], both materials are found electrified through the favorable adsorption of the solvated hydroxide ion but in a contrasting manner that gives full support to previous nanofluidics measurements and analysis [1, 27].

In this paper we undertake a screening of the possible border configurations when matching BN and G monolayer materials in a planar fashion. On all borders we first compute the dissociative adsorption of single water molecule in vacuum and corrected in a dielectric solvent in order to hint at the most favorable ones. On a few selected ones we run extensive Ab Initio Molecular Dynamics (AIMD) with an explicit interface with bulk water. On one border an interfacial H_2O molecule is found to spontaneously chemisorb onto one boron atom before dissociating by transferring a proton to the surrounding water. These reactive events occur within the few ps of the simulation unveiling the unexpected high reactivity of the hybrid composites.

RESULTS AND DISCUSSION

Static DFT study

As a start we considered all possible BN-G planar heterojunctions as candidates. The five different junctions and their labelling are displayed in Fig.**1**, and the corresponding simulation cells are displayed in Supplementary Figure 1. Note that each cell contains two border regions due to periodic boundary conditions. In the interface the border hexagons are necessarily a composite BCN one: for ZZ (AC) border there is an odd (even) number of each material. As a result we have considered the borders ZZ(B) and ZZ(N) and AC that are standard ones. For completeness we have also modelled the BinC and NinC junctions which comprise one single atom of each material. Notably in these junctions the border regions has an extended width of two hexagons while the border region is limited to one hexagon in any of the ZZ and AC edge geometries. To our knowledge the BinC and NinC junction have never been characterized experimentally and we denote them non-standard edges. For each junction, several H_2O dissociative adsorption configurations are possible and inspired by the previous studies [20, 26] we restrict them to the ones where i) the hydroxide is chemisorbed on a boron atom, ii) the proton is chemisorbed on a carbon atom, iii) the co-adsorption

View Article Online
DOI: 10.1039/C9CP06765E

occurs within the same hexagon in a cis conformation. The ii) choice is motivated by the exhaustive DFT study of Ref. [20] that shows C-H bonds are significantly stronger than N-H bonds when dissociating water on B-doped G and C-doped BN single layers. In total, 17 adsorption configurations are compared on 5 junction geometries and their dissociative adsorption energies are displayed in Fig. **2**. The dissociative adsorption energies of H_2O called E_{ads} on different edges were computed first in vacuum and second in implicit water at $T = 0$ K. To do so, the value of E_{ads} is obtained by comparing the total energy of the adsorbed ions on the surface $E_{ads/surf}$ with that of the flat pristine surface $E_{pristine}$ added to that of the pristine water molecule $E_{\mathrm{H_2O}}$ i.e. $E_{ads} = E_{ads/surf} - (E_{pristine} + E_{\mathrm{H_2O}})$. The adsorption energy calculation scheme is illustrated in Supplementary Figure 2.

E_{ads} on pristine atomic layers of BN and G were also included for comparison and yielded unfavorable dissociative adsorption energies above 2.5 eV (see Supplementary Table 1) in good agreement with previous results [20]. Also our AIMD study of water/BN and water/G interfaces with and without aqueous hydroxide ion gave no indication of water adsorption into these pristine layers. Indeed we showed differential adsorption of aqueous OH- at these interfaces in quantitative agreement with the measured negative surface charge, hence precluding co-adsorption of protons and consequently excluding water dissociation on the pristine layers. [26] As a general trend already observed in our previous static DFT study [28], the dissociative adsorption energies tend to be destabilized in implicit water versus in vacuum (see the orange triangles in the plot Fig. **2** are mostly lying in the energy scale below the blue circles). In some cases however the energy does not change too much when introducing a solvent correction. Our energetic results show that the non-standard edges - BinC and NinC on the left side of the plot in Fig. **2** - are more reactive towards water dissociative adsorption than the ZZ edges. AC configurations (right side) are globally the less reactive ones. Precisely, Fig. **2** exhibits three adsorbed configurations with negative (favorable) dissociative adsorption energies in the implicit water case: BinC Aa (-0.88 eV) and BinC Ba (-0.88 eV), and NinC Aa (-0.57 eV). These results corroborate the chemical enhancement effect of one-dimensional boundaries in 2D materials. Furthermore, the magnitude of the favourable adsorption energies indicate a strong interaction between the adsorbates and the surface, calling for more realistic dynamical quantum studies on the reactivity of H_2O at the liquid water / planar heterojunction interface, that we detail below.

View Article Online
DOI: 10.1039/C9CP06765E

Metastability of co-adsorbed hydroxide and proton by AIMD

Hydrogen bonds are of primordial importance for the water solvent. Therefore implicit solvation schemes can not fully satisfactorily describe the adsorption of H_2O fragments on BN and G atomic layers. In fact, the water self-ions OH^- and H^+ resulting from water auto-dissociation are transient species in water because they are subjected to fast proton transfers from H-bonded water molecules. In order to properly simulate such systems, one must resort to computationally expensive $ab-initio$ molecular dynamics (AIMD) simulations in which water molecules are comprehensively described. We therefore computed 10 ps long unbiased AIMD trajectories of several adsorption configurations in contact with 195 water molecules equilibrated at 323 K (see Methods). An example of an AIMD simulation cell without adsorbates is displayed in Fig. **3**. Due to computational costs only 4 of the 17 configurations could be tested by AIMD. The dissociated configurations tested by AIMD correspond to coloured (red and green) labels in Fig. **2**: the 3 configurations identified as favourable in implicit water by static DFT (BinC Aa, Ba and BinC Aa) and the most unfavourable dissociation configuration among the ZZ edges: ZZ(N) Ab. This last edge configuration corresponds to the experimentally observed junction geometry. In all 4 cases, the co-adsorbed fragments OH^- and H^+ were found metastable, as none of the adsorbed fragments was desorbing during the 10 ps of the dynamics. More interestingly the most unfavourable of the 4 configurations (ZZ(N) Ab) was also found metastable, despite a static adsorption energy computed as high as +1.97 eV. Hence it is likely that all of the 17 configurations considered in the present work would be found metastable if tested similarly i.e. by free AIMD simulations. This points out that the theoretical results originating solely from static DFT results might convey a partial picture of the reactivity in water solvent. This stresses even further the necessity of an explicit and quantum description of solvents like water at the interface of 2D materials.

Spontaneous Reaction

It is crucial to stress that the timescale and the number of chemical objects that one can simulate with AIMD do not allow for the observation of rare chemical events, so that one can only hope to witness extremely easy reactions along an unbiased trajectory. The

View Article Online
DOI: 10.1039/C9CP06765E

observation of any spontaneous reaction is therefore a strong indication of the extremely high reactivity of those surfaces. To better study the water dissociation mechanism, a water interface with a pristine NinC junction i.e. free of fragments, was thermalized at 323 K while preventing all water molecules to approach the surface below 2 Å. Upon release of the latter constraint, a water molecule starting at a large distance of 2.8 Å from the surface (see Fig. **4**a, cyan line) i.e. within the interfacial solvent layer (see the inset of Fig. **4**b, water density peak at 3.3 Å), was found to chemisorb on a boron atom of the junction after $t = 1.2$ ps of free MD (see Fig. **4**c, inset 2). The water adsorbates then rapidly dissociates into an adsorbed hydroxide and an aqueous hydronium at $t = 1.3$ ps (see Fig. **4**c, inset 3). Although the ions dynamically recombine transiently at certain points of the 10 ps long trajectory, the as created hydronium cation diffuses further away from the first solvation shell of the fixed adsorbed OH^-. To identify the dissociation state from the atomic configurations, we associate each hydrogen atom to the closest oxygen to it. The atoms with respectively one and three associated hydrogen are then defined as corresponding to the hydroxide and the hydronium. During the simulation the adsorbate is in a OH^- state only 94% of the time and in a H_2O state 6% of the remaining time.

The distance from the surface of the oxygen that adsorbs and the distance between the two water self-ions are respectively displayed in cyan and green in Fig. **4**a. The chaotic trajectory (green line) of the hydronium ion in water is simply the manifestation of its intrinsic reactivity in water: it will transfer one proton to a neighboring water that will become the hydronium species. This results into large diffusion jumps of the hydronium cation and blinking effects when tracking it in the dynamical simulation (see the whole 10 ps trajectory in Supplementary Movie 1).

We therefore propose a reaction in three steps, as illustrated in Fig. **4**c: diffusion of H_2O near the junction, chemisorption onto a border boron atom and subsequent but immediate dissociation. The last step indeed is seen to occur only once the adsorbed state reached, not during the approach of H_2O to the surface.

Starting from a different atomic configuration, another trajectory simulating the same reactive interface was computed for 21 ps. The chemisorption was once again observed - at $t = 2.5$ ps-, corroborating the likeliness of this reaction (see Supplementary Figure 3). Yet, although one proton of the adsorbates appears to be shared with a solvating water molecule, no clear dissociation occurs, i.e. with diffusion of the excess proton further than

View Article Online
DOI: 10.1039/C9CP06765E

the first solvation layer. With the method described above to identify the water self-ions from simulation, the adsorbate is in a OH^- state only 15% of the time and in a H_2O state 85% of the remaining time. Thus by comparing the two trajectories on the same junction starting with different solvent configuration, it appears that the organization of the solvation shell around the water adsorbate is playing a key role for its dissociation. This is expected from the strong role of solvent reorganisation in the proton diffusion process [21, 22] but is magnified here by sequential adsorption and dissociation processes. Further studies would be necessary to better understand how the solvent re-organization is coupled to these two events.

Taking into account periodic boundary conditions (PBC) of the simulation, the spontaneous dissociative adsorption of H_2O occurs at least once every 1.5 nm which corresponds to roughly 1/6 of the border boron sites being bonded to an oxygen atom. This estimate being based on the observation of the reaction in a limited time - 10 ps long AIMD trajectory-, we expect the actual occurrence to be much higher.

In the following, we aim at quantifying the reactivity of H_2O with the NinC junction by determining the free energy of adsorption of a water molecule. This was derived from the potential of mean force (PMF) obtained by umbrella sampling while moving the adsorbate away from the surface to the first interfacial layer of solvent by restraining the oxygen distance of the interacting water to the surface (see Methods). Because of the very high reactivity of the interface, preventing all other water molecules of the simulation cell from approaching the surface at less than 2 Å was proven necessary to avoid spontaneous adsorption. This is similar to constraining coordination numbers for the computation of pKa's to avoid unwanted re-protonation of the acid.[29, 30] The resulting free energy profile shown in Fig. **4**b displays a chemisorption well of - 43 meV located 1.6 Å away from the surface and a barrier of 90 meV at 2 Å. The basin around 3 Å corresponds to the water density peak of the first water layer at 3.3 Å from the surface. The minimum of this basin was taken as reference energy for the PMF (see Fig. **4**b, horizontal grey dotted line). Interestingly, the barrier height corresponds solely to about 4 k_BT, while a large number of potentially reacting molecules are present close to the junction as H_2O is the solvent, which furthermore displays a density peak in the vicinity of the surface.

How realistic are our predicted reactive junctions towards liquid water? Experimentally the observed ZZ border is mostly the ZZ(B) one [8, 15] and not the one that we found

View Article Online
DOI: 10.1039/C9CP06765E

highly reactive i.e. NinC. Hence we tested a similar reactivity at the ZZ(B) border [8, 15] by thermalizing, i.e. running MD at room temperature, a simulation cell consisting of one H_2O adsorbed on the border boron atom in plain water by restraining the adsorbed water molecule at 1.6 Å from the surface. Upon release of the latter restraint the water molecule was found to spontaneously desorb within a few hundreds of femtoseconds, as displayed in Supplementary Movie 2. Nevertheless, the adsorption configuration ZZ(B) Ba was also identified as metastable i.e the OH et H co-fragments remain stable during free MD (see previous section). Hence we postulate that the metastable adsorption state of the water fragment could be reached from ions already separated in solution or via concerted formation of the B-O bond and rupture of one O-H bond.

Nevertheless even if sharp 1D interfaces with NinC edge hexagons are not likely to be observed in planar heterojunctions, we infer that these asymmetric hexagons can still be present locally in a zero dimensionality of defects like G-doped BN and vice versa BN-doped graphene materials. Thus we hope that our results can forster such experiments to undertake a controlled reactivity study of environmental molecules on these composite BCN materials.

CONCLUSION

By means of ab initio calculations, we have evidenced a covalent chemistry on one water-immersed BN-G planar heterostructure, chemistry that does not exist on pristine materials. A large variety of border geometries were tested and the dissociative adsorption of H_2O to form B-OH^- and C-H^+ fragments was found energetically favorable in a few cases. One junction geometry was identified as particularly reactive with spontaneous adsorption of H_2O and subsequent dissociation into an adsorbed hydroxide and an aqueous hydronium. This reactive junction comprises one row of BN hexagons with one C atom substituting B and the next adjacent row of G hexagons with one N atom substituting C. Moreover such asymmetric composite hexagons echoe substitutional doping in 2D materials and hence may be also observed in patchy BN islands embedded in a graphene sheet and vice versa[5, 31]. The use of state-of-the-art techniques such as atomic force microscopy in water is an exquisite tool of choice to seek experimental evidence for the water adsorption and dissociation at the hBN-graphene junction. This unique tool requires an ultimate reduction of the noise and has been developed recently [32, 33]. We hope that our prediction will trigger more reactivity

View Article Online
DOI: 10.1039/C9CP06765E

studies on chemically doped 2D materials.

METHODS

Both DFT and AIMD simulations were performed using orthorhombic cells containing a hexagonal sheet consisting of 72 Carbon, 36 Boron and 36 Nitrogen atoms. To model the junctions of the zigzag and armchair type, 14.77 Å × 25.58 Å and 12.78 Å × 29.55 Å single layers were respectively used, separated by 15 Å of vacuum for static DFT calculations and 21 Å of explicit water for AIMD trajectories. The top views of the neutral Lewis structures of the three investigated cells are displayed in Supplementary Fig. 1a-c. The first and the second cell parameters are respectively parallel to the hybridised junction and perpendicular to the surface. The hBN and graphene primitive lattice parameters $\boldsymbol{a}$ (2.51 Å and 2.47 Å respectively) evaluated within the present DFT framework exhibit a mismatch of 0.04 Å, in agreement with previous calculations using a similar method[28, 34]. The lattice parameter of hBN was chosen to construct the cell, therefore inducing strain in the counterpart network. Because of the lattice mismatch, only a large supercell containing thousands surface atoms could prevent inducing strain in the layer. Static DFT calculations were performed using the Vienna Ab Initio Simulation Package (VASP) in its version 5.4.1, with a 800 eV cutoff of the plane-wave expansion of the wave functions. The electronic cores were described by pseudo-potentials under the projector augmented wave method [35]. The framework of the generalized gradient approximation (GGA) was used to evaluate exchange-correlation energies, with the so-called optPBE functional developed by Klimeš, Bowler and Michaelides [36]. The first Brillouin zone of the supercell was sampled at the gamma point. Solvation energies in implicit water were evaluated within the approach implemented into VASP by Mathew and Hennig [37]. In this scheme, the solvent is represented as a dielectric constant which is a functional of the electronic density, continuously spanning values from 0 to 80, the bulk water value asymptotically approached in regions where the electronic density is lower than $\rho_{cut} = 0.0025$ Å^3. All atomic configurations which energy was used to derive adsorption strengths were obtained after relaxing the structure to reach atomic forces below 0.05 eV/Å. A typical VASP input for a static DFT calculation with implicit water is shown in Supplementary Note 1.

AIMD was performed with the CP2K 5.1 code[38]. The forces were computed using density

View Article Online
DOI: 10.1039/C9CP06765E

functional theory (DFT) as implemented in the QuickStep module[39, 40]. Wavefunctions were projected over DZVP-MOLOPT-SR-GTH basis sets [41] and planewaves expanded to a 600 Ry energy cutoff. Geodecker-Teter-Hutter pseudopotentials were used to represent electronic cores [42–44]. The Perdew, Burke and Ernzerhof (PBE) functional was used[45] with the D3 dispersion correction scheme[46, 47]. In order to limit nuclear quantum effects and to reduce the time step size needed for energy conservation in our Born-Oppenheimer AIMD, the mass of all protons was substituted by that of deuterium. A time step of 0.5 fs was used for the dynamics. AIMD simulations were carried out in the NVT ensemble at 323 K using Nose-Hoover thermostats [48, 49] with a time constant of 500 fs. The PBE functional predicts a reasonable liquid water structure at this slightly increased temperature condition. The 21 Å high simulation cell contained 195 H_2O, yielding a pressure $<P> = 2 \pm 3$ MPa (see Supplementary Methods), and was built as follows. Using the Packmol software [50], the water molecules were randomly placed inside a 16 Å high cell which was later juxtaposed to the surface with a 2.5 Å vacuum separation between the hexagonal layer and the liquid. The system was heated up to 600 K before cooling down to 323.15 K, followed by a 3 ps equilibration. To test the metastability of the adsorbed state the two adsorbates were added to the simulation cell and restrained close to the surface for 2.5 ps before removal of the biases.

To obtain the potential of mean force of a water molecule close to the junction, the distance of one particular water oxygen to the surface was restrained using a harmonic bias with a force constant of 0.1 Ha/Bohr. This collective variable was defined as the oxygen distance to the closest surface atom. The target of the restraint was progressively moved from 1.4 Å to 3.6 Å along successive trajectories of 5 ps which starting point corresponds to 0.05 to 1 ps of the previous run. The two oxygen-hydrogen bond of the target H_2O were restrained by a harmonic potential centered at 1 Å with a force constant of 0.025 Ha/Bohr. Simultaneously, harmonic biases with a force constant of 0.1 Ha/Bohr were applied to each combination of another oxygen atom and any boron atom. The restraints were only applied when the oxygen-boron distance would come close to 2 Å in order to prevent spontaneous adsorptions. To define the collective variables and apply the biases, the open-source and community developed PLUMED library[51] was used in its version 2.4[52] as implemented in the CP2K 5.1 code. Typical CP2K and PLUMED input files used for biased dynamics can be respectively found in Supplementary Note 2 and Supplementary Note 3. Further

View Article Online
DOI: 10.1039/C9CP06765E

details regarding the PLUMED bias can be found in Supplementary Methods. To derive the free energy profile, the biased trajectories were analyzed using a home implementation of the Weighted Histogram Analysis Method (WHAM) developed by Kumar *et al.* [53] as formulated by Souailles and Roux in their extension of this protocol[54]. A bin size of 0.05 Å was choose to compute the histograms. Evidence of convergence of the WHAM analysis used to derive the PMF of Fig. **4**b is displayed in Supplementary Figure 4. The final snapshot of the trajectory with the H_2O restrained at 3.2 (3.0) Å from the surface was used as starting point for the bias-free trajectory leading to spontaneous adsorption of a water molecule, with (without) further dissociation. The water density profile displayed in inset in Fig. **4**b was evaluated over 30 ps of trajectory corresponding to the gathering of the two simulations of the NinC junction in water. More detailed profiles are displayed in Supplementary Figure 5.

REFERENCES

[1] Siria, A. *et al.* Giant osmotic energy conversion measured in a single transmembrane boron nitride nanotube. *Nature* **494**, 455–458 (2013).

[2] Siria, A., Bocquet, M.-L. & Bocquet, L. New avenues for the large-scale harvesting of blue energy. *Nat. Rev. Chem.* **1**, 0091 (2017).

[3] Ci, L. *et al.* Atomic layers of hybridized boron nitride and graphene domains. *Nat. Mater.* **9**, 430–435 (2010).

[4] Hus, S. M. & Li, A.-P. Spatially-resolved studies on the role of defects and boundaries in electronic behavior of 2D materials. *Prog. Surf. Sci.* **92**, 176–201 (2017).

[5] Chen, S. *et al.* Designing boron nitride islands in carbon materials for efficient electrochemical synthesis of hydrogen peroxide. *J. Am. Chem. Soc.* **140**, 7851–7859 (2018).

[6] Levendorf, M. P. *et al.* Graphene and boron nitride lateral heterostructures for atomically thin circuitry. *Nature* **488**, 627–632 (2012).

[7] Kim, S. M. *et al.* Synthesis of patched or stacked graphene and hBN flakes: A route to hybrid structure discovery. *Nano Lett.* **13**, 933–941 (2013).

[8] Han, G. H. *et al.* Continuous growth of hexagonal graphene and boron nitride in-plane heterostructures by atmospheric pressure chemical vapor deposition. *ACS Nano* **7**, 10129–10138

View Article Online
DOI: 10.1039/C9CP06765E

(2013).

[9] Liu, L. *et al.* Heteroepitaxial growth of two-dimensional hexagonal boron nitride templated by graphene edges. *Science* **343**, 163–167 (2014). URL `https://doi.org/10.1126%2Fscience.1246137`.

[10] Zhuang, P. *et al.* Growth of lateral graphene/h-BN heterostructure on copper foils by chemical vapor deposition. *Nanotechnology* **30**, 03LT01 (2018).

[11] Sutter, P., Cortes, R., Lahiri, J. & Sutter, E. Interface formation in monolayer graphene-boron nitride heterostructures. *Nano Lett.* **12**, 4869–4874 (2012).

[12] Sutter, P., Huang, Y. & Sutter, E. Nanoscale integration of two-dimensional materials by lateral heteroepitaxy. *Nano Lett.* **14**, 4846–4851 (2014).

[13] Liu, M. *et al.* Quasi-freestanding monolayer heterostructure of graphene and hexagonal boron nitride on ir(111) with a zigzag boundary. *Nano Lett.* **14**, 6342–6347 (2014).

[14] Gao, Y. *et al.* Toward single-layer uniform hexagonal boron nitride–graphene patchworks with zigzag linking edges. *Nano Lett.* **13**, 3439–3443 (2013).

[15] Drost, R. *et al.* Electronic states at the graphene–hexagonal boron nitride zigzag interface. *Nano Lett.* **14**, 5128–5132 (2014).

[16] Petrović, M., von Hoegen, M. H. & zu Heringdorf, F.-J. M. Lateral heterostructures of hexagonal boron nitride and graphene: BCN alloy formation and microstructuring mechanism. *Appl. Surf. Sci.* **455**, 1086–1094 (2018).

[17] Nguyen, T. H. *et al.* Microscopic insight into the single step growth of in-plane heterostructures between graphene and hexagonal boron nitride. *Adv. Mater. Interfaces* **12**, 675–682 (2019).

[18] Zhang, S., Li, J., Wu, H., Li, X. & Guo, W. Direct synthesizing in-plane heterostructures of graphene and hexagonal boron nitride in designed pattern. *Adv. Mater. Interfaces* **5**, 1800208 (2018).

[19] Sun, Q., Sun, C., Du, A., Dou, S. & Li, Z. In-plane graphene/boron-nitride heterostructures as an efficient metal-free electrocatalyst for the oxygen reduction reaction. *Nanoscale* **8**, 14084–14091 (2016).

[20] Al-Hamdani, Y. S., Alfè, D., von Lilienfeld, O. A. & Michaelides, A. Tuning dissociation using isoelectronically doped graphene and hexagonal boron nitride: Water and other small molecules. *J. Chem. Phys.* **144**, 154706 (2016).

View Article Online
DOI: 10.1039/C9CP06765E

[21] Tuckerman, M., Laasonen, K., Sprik, M. & Parrinello, M. Ab initio molecular dynamics simulation of the solvation and transport of hydronium and hydroxyl ions in water. *J. Chem. Phys.* **103**, 150–161 (1995).

[22] Tuckerman, M., Laasonen, K., Sprik, M. & Parrinello, M. Ab Initio Molecular Dynamics Simulation of the Solvation and Transport of H3o+ and OH- Ions in Water. *J. Phys. Chem.* **99**, 5749–5752 (1995).

[23] Chen, M. *et al.* Hydroxide diffuses slower than hydronium in water because its solvated structure inhibits correlated proton transfer. *Nat. Chem.* **10**, 413–419 (2018).

[24] Cheng, J. & Sprik, M. Acidity of the Aqueous Rutile TiO2(110) Surface from Density Functional Theory Based Molecular Dynamics. *J. Chem. Theory Comput.* **6**, 880–889 (2010).

[25] Tazi, S., Rotenberg, B., Salanne, M., Sprik, M. & Sulpizi, M. Absolute acidity of clay edge sites from ab-initio simulations. *Geochimica et Cosmochimica Acta* **94**, 1–11 (2012).

[26] Grosjean, B., Bocquet, M.-L. & Vuilleumier, R. Versatile electrification of two-dimensional nanomaterials in water. *Nat. Comm.* **10** (2019).

[27] Secchi, E., Niguès, A., Jubin, L., Siria, A. & Bocquet, L. Scaling behavior for ionic transport and its fluctuations in individual carbon nanotubes. *Phys. Rev. Lett.* **116**, 154501 (2016).

[28] Grosjean, B. *et al.* Chemisorption of hydroxide on 2D materials from DFT calculations: Graphene versus hexagonal boron nitride. *J. Phys. Chem. Lett.* **7**, 4695–4700 (2016).

[29] Sprik, M. Coordination numbers as reaction coordinates in constrained molecular dynamics. *Faraday Discussions* **110**, 437–445 (1998).

[30] Sprik, M. Computation of the pK of liquid water using coordination constraints. *Chemical Physics* **258**, 139–150 (2000).

[31] Lu, J. *et al.* Order–disorder transition in a two-dimensional boron–carbon–nitride alloy. *Nat. Comm.* **4** (2013).

[32] Schlesinger, I., Kuchuk, K. & Sivan, U. An ultra-low noise optical head for liquid environment atomic force microscopy. *Rev. Sci. Instrum.* **86**, 083705 (2015).

[33] Kuchuk, K. & Sivan, U. Hydration structure of a single DNA molecule revealed by frequency-modulation atomic force microscopy. *Nano Lett.* **18**, 2733–2737 (2018).

[34] Graziano, G., Klimeš, J., Fernandez-Alonso, F. & Michaelides, A. Improved description of soft layered materials with van der waals density functional theory. *J. Phys.: Condens. Matter* **24**, 424216 (2012).

View Article Online
DOI: 10.1039/C9CP06765E

[35] Kresse, G. & Joubert, D. From ultrasoft pseudopotentials to the projector augmented-wave method. *Phys. Rev. B* **59**, 1758–1775 (1999).

[36] Klimeš, J., Bowler, D. R. & Michaelides, A. Chemical accuracy for the van der waals density functional. *J. Phys.: Condens. Matter* **22**, 022201 (2009).

[37] Mathew, K., Sundararaman, R., Letchworth-Weaver, K., Arias, T. A. & Hennig, R. G. Implicit solvation model for density-functional study of nanocrystal surfaces and reaction pathways. *J. Chem. Phys.* **140**, 084106 (2014).

[38] Hutter, J., Iannuzzi, M., Schiffmann, F. & VandeVondele, J. CP2K: atomistic simulations of condensed matter systems. *Wiley Interdiscip. Rev. Comput. Mol. Sci.* **4**, 15–25 (2013).

[39] VandeVondele, J. *et al.* Quickstep: Fast and accurate density functional calculations using a mixed Gaussian and plane waves approach. *Comput. Phys. Commun.* **167**, 103–128 (2005).

[40] Lippert, G., Hutter, J. & Parrinello, M. A hybrid gaussian and plane wave density functional scheme. *Mol. Phys.* **92**, 477–488 (1997).

[41] VandeVondele, J. & Hutter, J. Gaussian basis sets for accurate calculations on molecular systems in gas and condensed phases. *J. Chem. Phys.* **127**, 114105 (2007).

[42] Goedecker, S., Teter, M. & Hutter, J. Separable Dual-Space Gaussian Pseudopotentials. *Phys. Rev. B* **54**, 1703–1710 (1996).

[43] Hartwigsen, C., Goedecker, S. & Hutter, J. Relativistic separable dual-space Gaussian pseudopotentials from H to Rn. *Phys. Rev. B* **58**, 3641–3662 (1998).

[44] Krack, M. Pseudopotentials for H to Kr optimized for gradient-corrected exchange-correlation functionals. *Theor. Chem. Acc.* **114**, 145–152 (2005).

[45] Perdew, J. P., Burke, K. & Ernzerhof, M. Generalized gradient approximation made simple. *Phys. Rev. Lett.* **77**, 3865–3868 (1996).

[46] Grimme, S., Antony, J., Ehrlich, S. & Krieg, H. A consistent and accurate ab initio parametrization of density functional dispersion correction (DFT-d) for the 94 elements H-Pu. *J. Chem. Phys.* **132**, 154104 (2010).

[47] Grimme, S., Ehrlich, S. & Goerigk, L. Effect of the damping function in dispersion corrected density functional theory. *J. Comput. Chem.* **32**, 1456–1465 (2011).

[48] Nosé, S. A molecular dynamics method for simulations in the canonical ensemble. *Mol. Phys.* **52**, 255–268 (1984).

View Article Online
DOI: 10.1039/C9CP06765E

[49] Nosé, S. A unified formulation of the constant temperature molecular dynamics methods. *J. Chem. Phys.* **81**, 511–519 (1984).

[50] Martinez, L., Andrade, R., Birgin, E. G. & Martinez, J. M. PACKMOL: A package for building initial configurations for molecular dynamics simulations. *J. Comput. Chem.* **30**, 2157–2164 (2009).

[51] The PLUMED consortium: A community effort to promote openness, transparency and reproducibility in molecular simulations (Submitted).

[52] Tribello, G. A., Bonomi, M., Branduardi, D., Camilloni, C. & Bussi, G. PLUMED 2: New feathers for an old bird. *Comput. Phys. Commun.* **185**, 604–613 (2014).

[53] Kumar, S., Rosenberg, J. M., Bouzida, D., Swendsen, R. H. & Kollman, P. A. The weighted histogram analysis method for free-energy calculations on biomolecules. *J. Comput. Chem.* **13**, 1011–1021 (1992).

[54] Souaille, M. & Roux, B. Extension to the weighted histogram analysis method: combining umbrella sampling with free energy calculations. *Comput. Phys. Commun.* **135**, 40–57 (2001).

[55] Siria, A. *et al.* Giant osmotic energy conversion measured in a single transmembrane boron nitride nanotube. *Nature* **494**, 455–458 (2013).

[56] Siria, A., Bocquet, M.-L. & Bocquet, L. New avenues for the large-scale harvesting of blue energy. *Nat. Rev. Chem.* **1**, 0091 (2017).

[57] Ci, L. *et al.* Atomic layers of hybridized boron nitride and graphene domains. *Nat. Mater.* **9**, 430–435 (2010).

[58] Hus, S. M. & Li, A.-P. Spatially-resolved studies on the role of defects and boundaries in electronic behavior of 2D materials. *Prog. Surf. Sci.* **92**, 176–201 (2017).

[59] Chen, S. *et al.* Designing boron nitride islands in carbon materials for efficient electrochemical synthesis of hydrogen peroxide. *J. Am. Chem. Soc.* **140**, 7851–7859 (2018).

[60] Levendorf, M. P. *et al.* Graphene and boron nitride lateral heterostructures for atomically thin circuitry. *Nature* **488**, 627–632 (2012).

[61] Kim, S. M. *et al.* Synthesis of patched or stacked graphene and hBN flakes: A route to hybrid structure discovery. *Nano Lett.* **13**, 933–941 (2013).

[62] Han, G. H. *et al.* Continuous growth of hexagonal graphene and boron nitride in-plane heterostructures by atmospheric pressure chemical vapor deposition. *ACS Nano* **7**, 10129–10138 (2013).

View Article Online
DOI: 10.1039/C9CP06765E

[63] Liu, L. *et al.* Heteroepitaxial growth of two-dimensional hexagonal boron nitride templated by graphene edges. *Science* **343**, 163–167 (2014). URL `https://doi.org/10.1126%2Fscience.1246137`.

[64] Zhuang, P. *et al.* Growth of lateral graphene/h-BN heterostructure on copper foils by chemical vapor deposition. *Nanotechnology* **30**, 03LT01 (2018).

[65] Sutter, P., Cortes, R., Lahiri, J. & Sutter, E. Interface formation in monolayer graphene-boron nitride heterostructures. *Nano Lett.* **12**, 4869–4874 (2012).

[66] Sutter, P., Huang, Y. & Sutter, E. Nanoscale integration of two-dimensional materials by lateral heteroepitaxy. *Nano Lett.* **14**, 4846–4851 (2014).

[67] Liu, M. *et al.* Quasi-freestanding monolayer heterostructure of graphene and hexagonal boron nitride on ir(111) with a zigzag boundary. *Nano Lett.* **14**, 6342–6347 (2014).

[68] Gao, Y. *et al.* Toward single-layer uniform hexagonal boron nitride–graphene patchworks with zigzag linking edges. *Nano Lett.* **13**, 3439–3443 (2013).

[69] Drost, R. *et al.* Electronic states at the graphene–hexagonal boron nitride zigzag interface. *Nano Lett.* **14**, 5128–5132 (2014).

[70] Petrović, M., von Hoegen, M. H. & zu Heringdorf, F.-J. M. Lateral heterostructures of hexagonal boron nitride and graphene: BCN alloy formation and microstructuring mechanism. *Appl. Surf. Sci.* **455**, 1086–1094 (2018).

[71] Nguyen, T. H. *et al.* Microscopic insight into the single step growth of in-plane heterostructures between graphene and hexagonal boron nitride. *Adv. Mater. Interfaces* **12**, 675–682 (2019).

[72] Zhang, S., Li, J., Wu, H., Li, X. & Guo, W. Direct synthesizing in-plane heterostructures of graphene and hexagonal boron nitride in designed pattern. *Adv. Mater. Interfaces* **5**, 1800208 (2018).

[73] Sun, Q., Sun, C., Du, A., Dou, S. & Li, Z. In-plane graphene/boron-nitride heterostructures as an efficient metal-free electrocatalyst for the oxygen reduction reaction. *Nanoscale* **8**, 14084–14091 (2016).

[74] Al-Hamdani, Y. S., Alfè, D., von Lilienfeld, O. A. & Michaelides, A. Tuning dissociation using isoelectronically doped graphene and hexagonal boron nitride: Water and other small molecules. *J. Chem. Phys.* **144**, 154706 (2016).

[75] Tuckerman, M., Laasonen, K., Sprik, M. & Parrinello, M. Ab initio molecular dynamics simulation of the solvation and transport of hydronium and hydroxyl ions in water. *J. Chem.*

View Article Online
DOI: 10.1039/C9CP06765E

Phys. **103**, 150–161 (1995).

[76] Tuckerman, M., Laasonen, K., Sprik, M. & Parrinello, M. Ab Initio Molecular Dynamics Simulation of the Solvation and Transport of H3o+ and OH- Ions in Water. *J. Phys. Chem.* **99**, 5749–5752 (1995).

[77] Chen, M. *et al.* Hydroxide diffuses slower than hydronium in water because its solvated structure inhibits correlated proton transfer. *Nat. Chem.* **10**, 413–419 (2018).

[78] Cheng, J. & Sprik, M. Acidity of the Aqueous Rutile TiO2(110) Surface from Density Functional Theory Based Molecular Dynamics. *J. Chem. Theory Comput.* **6**, 880–889 (2010).

[79] Tazi, S., Rotenberg, B., Salanne, M., Sprik, M. & Sulpizi, M. Absolute acidity of clay edge sites from ab-initio simulations. *Geochimica et Cosmochimica Acta* **94**, 1–11 (2012).

[80] Grosjean, B., Bocquet, M.-L. & Vuilleumier, R. Versatile electrification of two-dimensional nanomaterials in water. *Nat. Comm.* **10** (2019).

[81] Secchi, E., Niguès, A., Jubin, L., Siria, A. & Bocquet, L. Scaling behavior for ionic transport and its fluctuations in individual carbon nanotubes. *Phys. Rev. Lett.* **116**, 154501 (2016).

[82] Grosjean, B. *et al.* Chemisorption of hydroxide on 2D materials from DFT calculations: Graphene versus hexagonal boron nitride. *J. Phys. Chem. Lett.* **7**, 4695–4700 (2016).

[83] Sprik, M. Coordination numbers as reaction coordinates in constrained molecular dynamics. *Faraday Discussions* **110**, 437–445 (1998).

[84] Sprik, M. Computation of the pK of liquid water using coordination constraints. *Chemical Physics* **258**, 139–150 (2000).

[85] Lu, J. *et al.* Order–disorder transition in a two-dimensional boron–carbon–nitride alloy. *Nat. Comm.* **4** (2013).

[86] Schlesinger, I., Kuchuk, K. & Sivan, U. An ultra-low noise optical head for liquid environment atomic force microscopy. *Rev. Sci. Instrum.* **86**, 083705 (2015).

[87] Kuchuk, K. & Sivan, U. Hydration structure of a single DNA molecule revealed by frequency-modulation atomic force microscopy. *Nano Lett.* **18**, 2733–2737 (2018).

[88] Graziano, G., Klimeš, J., Fernandez-Alonso, F. & Michaelides, A. Improved description of soft layered materials with van der waals density functional theory. *J. Phys.: Condens. Matter* **24**, 424216 (2012).

[89] Kresse, G. & Joubert, D. From ultrasoft pseudopotentials to the projector augmented-wave method. *Phys. Rev. B* **59**, 1758–1775 (1999).

View Article Online
DOI: 10.1039/C9CP06765E

[90] Klimeš, J., Bowler, D. R. & Michaelides, A. Chemical accuracy for the van der waals density functional. *J. Phys.: Condens. Matter* **22**, 022201 (2009).

[91] Mathew, K., Sundararaman, R., Letchworth-Weaver, K., Arias, T. A. & Hennig, R. G. Implicit solvation model for density-functional study of nanocrystal surfaces and reaction pathways. *J. Chem. Phys.* **140**, 084106 (2014).

[92] Hutter, J., Iannuzzi, M., Schiffmann, F. & VandeVondele, J. CP2K: atomistic simulations of condensed matter systems. *Wiley Interdiscip. Rev. Comput. Mol. Sci.* **4**, 15–25 (2013).

[93] VandeVondele, J. *et al.* Quickstep: Fast and accurate density functional calculations using a mixed Gaussian and plane waves approach. *Comput. Phys. Commun.* **167**, 103–128 (2005).

[94] Lippert, G., Hutter, J. & Parrinello, M. A hybrid gaussian and plane wave density functional scheme. *Mol. Phys.* **92**, 477–488 (1997).

[95] VandeVondele, J. & Hutter, J. Gaussian basis sets for accurate calculations on molecular systems in gas and condensed phases. *J. Chem. Phys.* **127**, 114105 (2007).

[96] Goedecker, S., Teter, M. & Hutter, J. Separable Dual-Space Gaussian Pseudopotentials. *Phys. Rev. B* **54**, 1703–1710 (1996).

[97] Hartwigsen, C., Goedecker, S. & Hutter, J. Relativistic separable dual-space Gaussian pseudopotentials from H to Rn. *Phys. Rev. B* **58**, 3641–3662 (1998).

[98] Krack, M. Pseudopotentials for H to Kr optimized for gradient-corrected exchange-correlation functionals. *Theor. Chem. Acc.* **114**, 145–152 (2005).

[99] Perdew, J. P., Burke, K. & Ernzerhof, M. Generalized gradient approximation made simple. *Phys. Rev. Lett.* **77**, 3865–3868 (1996).

[100] Grimme, S., Antony, J., Ehrlich, S. & Krieg, H. A consistent and accurate ab initio parametrization of density functional dispersion correction (DFT-d) for the 94 elements H-Pu. *J. Chem. Phys.* **132**, 154104 (2010).

[101] Grimme, S., Ehrlich, S. & Goerigk, L. Effect of the damping function in dispersion corrected density functional theory. *J. Comput. Chem.* **32**, 1456–1465 (2011).

[102] Nosé, S. A molecular dynamics method for simulations in the canonical ensemble. *Mol. Phys.* **52**, 255–268 (1984).

[103] Nosé, S. A unified formulation of the constant temperature molecular dynamics methods. *J. Chem. Phys.* **81**, 511–519 (1984).

View Article Online
DOI: 10.1039/C9CP06765E

[104] Martinez, L., Andrade, R., Birgin, E. G. & Martinez, J. M. PACKMOL: A package for building initial configurations for molecular dynamics simulations. *J. Comput. Chem.* **30**, 2157–2164 (2009).

[105] The PLUMED consortium: A community effort to promote openness, transparency and reproducibility in molecular simulations (Submitted).

[106] Tribello, G. A., Bonomi, M., Branduardi, D., Camilloni, C. & Bussi, G. PLUMED 2: New feathers for an old bird. *Comput. Phys. Commun.* **185**, 604–613 (2014).

[107] Kumar, S., Rosenberg, J. M., Bouzida, D., Swendsen, R. H. & Kollman, P. A. The weighted histogram analysis method for free-energy calculations on biomolecules. *J. Comput. Chem.* **13**, 1011–1021 (1992).

[108] Souaille, M. & Roux, B. Extension to the weighted histogram analysis method: combining umbrella sampling with free energy calculations. *Comput. Phys. Commun.* **135**, 40–57 (2001).

CONFLICS OF INTEREST

There are no conflicts of interest to declare.

ACKNOWLEDGEMENTS

This work was performed on the French national supercomputer Occigen under the DARI grants A0030807364 and A0030802309. M.L.B acknowlegdes funding from the EU H2020 Framework Programme/ERC Advanced Grant agreement number 785911—Shadoks.

View Article Online
DOI: 10.1039/C9CP06765E

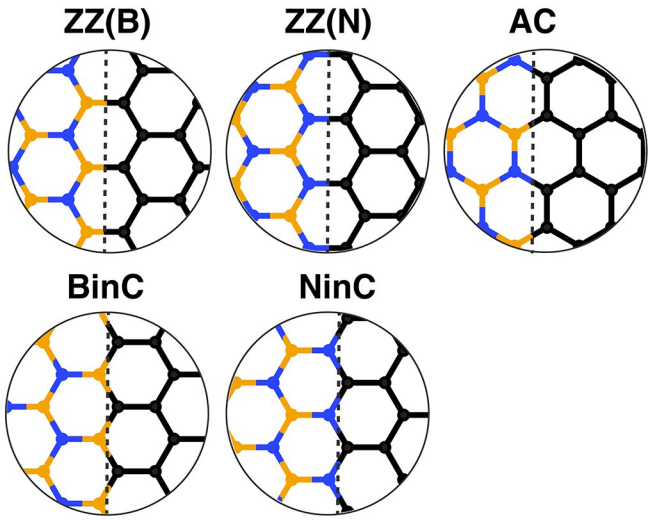

Figure 1. Possible junction geometries for the planar heterostructure and their acronyms. ZZ (AC) stands for zigzag (armchair) edges where the composite hexagons comprises 3 (4 or 2) atoms from BN and 3 (2 or 4) atoms from GR. For the zigzag boundaries, there is either a C-B interfacial bond called ZZ(B) or a C-N bond called ZZ(N). The junctions BinC and NinC correspond to a composite hexagon formed with one single atom B and N respectively from BN and the rest from GR.The junction line is schematically represented by a black dotted line while the boron, carbon and nitrogen atoms are respectively displayed in orange, black and blue.

View Article Online
DOI: 10.1039/C9CP06765E

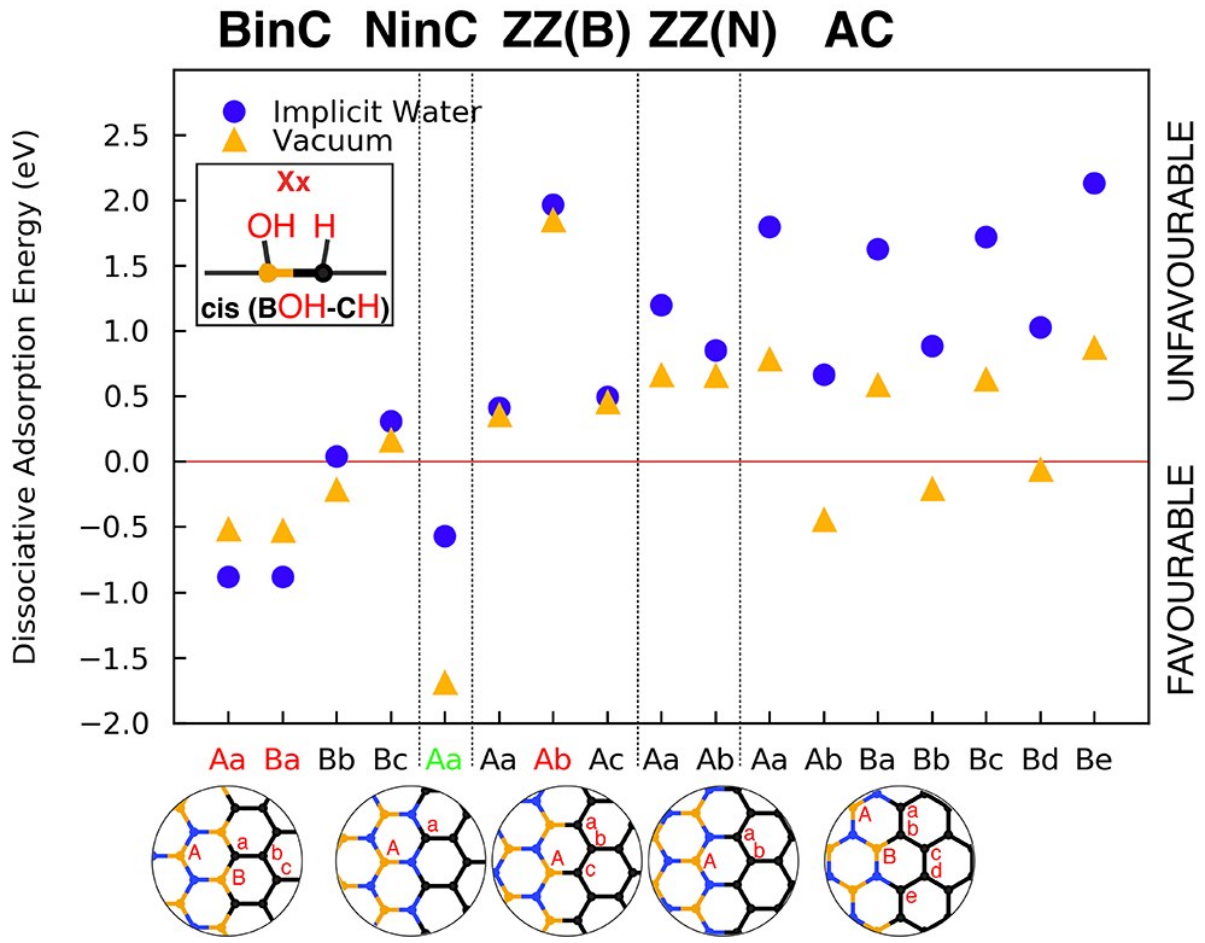

Figure 2. Static DFT H_2O Dissociative Adsorption Energies limited to OH fragment bonded to a boron atom while H fragment bonded to a carbon atom in the same composite hexagon of the heterostructure. Dissociative adsorption energies of H_2O in vacuum (orange triangles) and implicit water (blue circles) for various adsorption configurations on 5 distinct junction geometries defined in Fig. **1**. Red uppercase letters label hydroxide adsorption sites while red lowercase letters indicate associated proton adsorption sites. Coloured labels indicate configuration which meta-stability was also tested in explicit water by ab-initio molecular dynamics. Spontaneous dissociative adsorption of H_2O was observed on the green labelled geometry.

View Article Online
DOI: 10.1039/C9CP06765E

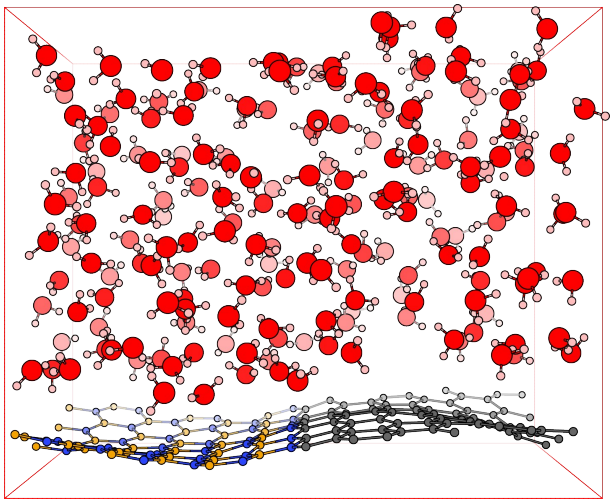

Figure 3. **Ab Initio Molecular Dynamics Simulation Cell.** Example of simulation cell with explicit water. The NinC junction geometry is represented along with 195 H_2O. Hydrogen, boron, carbon, nitrogen and oxygen atoms are respectively represented in pink, orange, grey, blue and red.

558 :

View Article Online
DOI: 10.1039/C9CP06765E

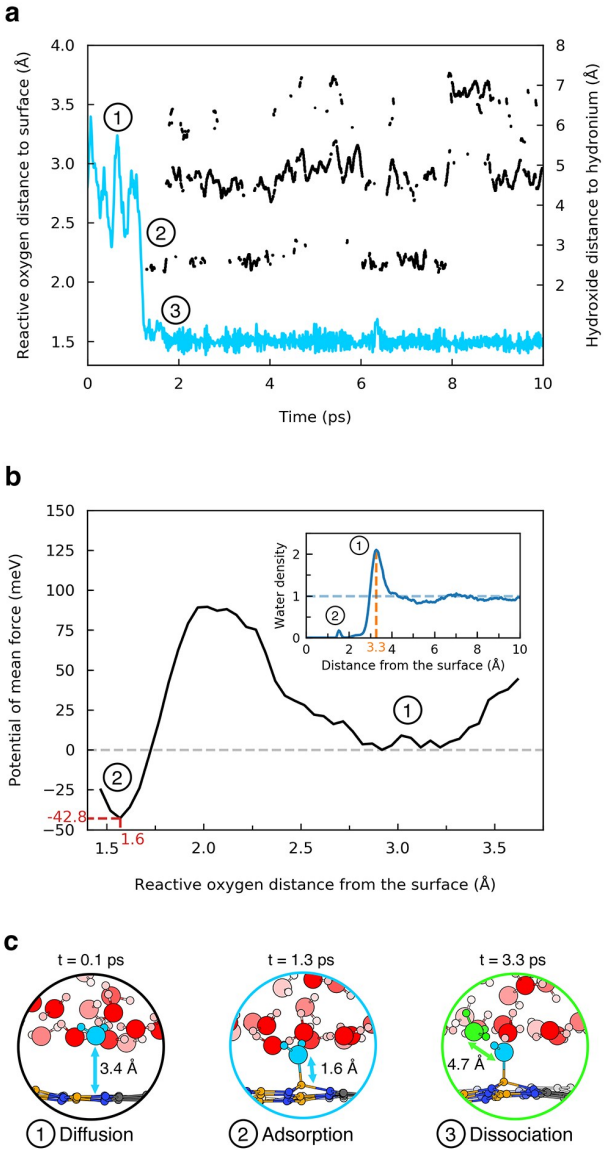

Figure 4. **Spontaneous Dissociative Adsorption of Water.** 10 ps long bias-free AIMD simulation of the NinC junction in water leading to the observation of a water dissociative adsorption. **a)** The distance to the surface of the oxygen adsorbing on a boron atom and the distance between the dissociated OH^- and H_3O^+ are respectively represented by a cyan line and black dots along the trajectory. **b)** Potential of mean force of a H_2O with respect to its distance to the surface (black line), with the energy reference represented by a grey dotted horizontal line. The energy and position of the chemisorption well is indicated in red. (inset: The water density with respect to the distance of the surface with the horizontal and vertical lines respectively indicating the bulk density value and the position of the interfacial layer. The density corresponds to an average over the whole cell.) **c)** Snapshots of the dynamics with associated times and distances. The reactive H_2O and OH^- are both represented in cyan. Circled numbers correspond to the ones in **a** and **b**.